Numerical simulation of microflow over superhydrophobic surfaces by lattice Boltmann method

Wenning ZHOU, Yuying YAN*
Faculty of Engineering, University of Nottingham, University Park, NG7 2RD, UK
*Corresponding to yuying.yan@nottingham.ac.uk, Tel: +44 (0) 115 951 3168

Abstract The superhydrophobicity of a microchannel is determined by not only the wettability of channel wall but also the surface topography. Recent experiments have found that superhrydrophobic surfaces can be achieved by pattering roughness on hydrophobic surfaces. In this paper, the dynamics of two-phase flow in microchannel with different wettability and topography is studied numerically by the lattice Boltzmann method (LBM). The mechanism of drag reduction resulted from the superhydrophobicity is investigated. In particular, the effect of different rough surfaces on superhydrophobicity is analyzed. It is found that flow behaviours are strongly affected by the wall wettability and topography. The results show that the LBM has a good application prospect in the study of drag reduction in microchannels.

Key words: microchannel, two-phase flow, lattice Boltzmann method, wettablity, superhydrophobicity.

1. Introduction

Since the lotus effect on self-cleaning was discovered, many discussions have been made and more and more attention has been paid to surface wettabilities, such as the hydrophilic, hydrophobic and superhydrophobic surfaces. In particular, superhydrophobic surfaces have attracted great interest due to their water-repellent and self-cleaning properties (Yan, 2009). It is well known that the surface wettablility is mainly determined by its surface free energy. The superhydrophobic surface is usually designed with low surface free energy materials. However, the micro- and/or nano-structures also play a role in determining the surface wettability. The method of chemical surface modification can only make a contact angle to be as large as 120°. To achieve a superhydrophobic surface which should have a contact angle of larger than 150°, the second factor mentioned above has to be considered. So far, much experimental work has been carried out, in which superhydrophobic surfaces can be achieved by patterning micro-structures on the hydrophobic surfaces. Apparent drop of pressure can be seen when fluid flow in these channels with superhydrophobic surfaces. Meanwhile, many theoretical and numerical studies have also been carried out. The wettablity of patterned surfaces is investigated by using the lattice Boltzmann method (LBM) (Dupuis and Yeomans, 2004; Yan and Zu, 2007; Zu et al., 2010). The effect of obstacles in microchannels on the process of capillary filling is investigated by LBM as well as CFD and MD approach (Chibbaro et al., 2009). The movement of contact line on heterogeneous surfaces was also studied by using a mean-field free-energy lattice Boltzmann method in (Zhang and Kwok, 2006). A model was proposed by (Gao and Yan, 2009), which combines both factors caused by surface structure and energy change. They found that Cassie-Baxter equation should be adopted when considering the hierarchical rough surface. However, all the above studies are not for flows. Recently, fluid flow on the superhydrophobic surfaces is simulated in (Cui et al., 2010). The drag reduction is also analyzed in their work. However, the effect of the style of roughness is not examined. In hydrodynamic systems with superhydrophobic surfaces, the surface roughness has great effect on fluid flow dynamics.

Thus, the aim of the present study is to

examine the effect of surface roughness on fluid flow by the LBM. As a mesoscopic approach, the LBM possesses many advantages over the traditional computational fluid dynamics approaches, such as simply to implement, easy to deal with the complex boundary conditions and high parallelism. Moreover, the ability to incorporate the microscopic interactions makes lattice Boltzmann method capable in simulating multiphase and micro-flow. Several models have been proposed for modeling multiphase fluid flow in the past years. Among them, three models are mostly used in multiphase flow simulations, namely chromodynamic model, the Shan-Chen model and the free-energy model. There are already several good reviews of these models, such as (Chen and Doolen, 1998). In this study, the Shan-Chen model is employed due to its ability to separate the interface automatically and easiness to implement the different wettabilty conditions.

2. Numerical method

2.1 The basic LBM

Basically, the LBM considers fluid as many fictitious particles; and by employing some rules on these particles, the fluid dynamics can be macroscopically obtained (Yan et al., 2010). The model is carried out through two basic steps on the particle distribution functions including the collision step and the streaming step, which can be written by the following form

$$f_i(x+c_i\Delta t,t+\Delta t)=f_i(x,t)-\frac{1}{\tau}(f_i(x,t)-f_i^{eq}(x,t)) \tag{1}$$

where τ is the dimensional relaxation time, $f_i(x,t)$ is the particle distribution function for the particle moving with velocity c_i at position x and time t, and $f_i^{eq}(x,t)$ is the local equilibrium distribution function. For the typical two-dimensional nine-speed (D2Q9) lattice scheme considered in the present work, the local equilibrium distribution function is defined as

$$f_i^{(eq)}=\rho w_i[1+\frac{c_i\cdot u}{c_s^2}+\frac{(c_i\cdot u)^2}{2c_s^4}-\frac{u\cdot u}{2c_s^2}] \tag{2}$$

where w_i is weighting factor, given as 4/9 for i =0, 1/9 for i =1,2,3,4, and 1/36 for i =5,6,7,8. c_s is the sound speed. c_i is the discrete velocities, and defined as

$$c_i=\begin{cases}(0,0), i=0\\ c(\cos\theta_i,\sin\theta_i),(\theta_i=(i-1)\pi/2, i=1,2,3,4)\\ \sqrt{2}c(\cos\theta_i,\sin\theta_i),(\theta_i=(i-5)\pi/2+\pi/4, i=5,6,7,8)\end{cases} \tag{3}$$

where $c=\Delta x/\Delta t$ is the particle streaming speed. Δx, Δt are the lattice spacing and time step. The relation between c_s and c can be expressed as $c_s=c/\sqrt{3}$. The macroscopic variables such as the mass density, the momentum density and the pressure are defined by sums over the distribution functions $f_i(x,t)$

$$\rho=\sum_i f_i,\quad \rho u=\sum_i f_i c_i,\quad p=\frac{c^2}{3}\rho \tag{4}$$

2.2 Shan- Chen model

In Shan-Chen's multiphase or multi-component model, one distribution function is introduced for each component. The particle distribution functions of each component satisfies the following equation

$$f_i^{\sigma}(x+c_i\Delta t,t+\Delta t)=f_i^{\sigma}(x,t)-\frac{1}{\tau^{\sigma}}(f_i^{\sigma}(x,t)-f_i^{\sigma,eq}(x,t)) \tag{5}$$

where $f_i^{\sigma}(x,t)$ is the σ th component density distribution function and τ^{σ} is a relaxation time of the σ th component which is related to its viscosity as $v^{\sigma}=c_s^2(\tau^{\sigma}-0.5\Delta t)$. The equilibrium distribution function $f_i^{\sigma,eq}(x,t)$ can be calculated as

$$f_i^{\sigma,eq}=\rho_{\sigma}w_i[1+\frac{c_i\cdot u_{\sigma}^{eq}}{c_s^2}+\frac{(c_i\cdot u_{\sigma}^{eq})^2}{2c_s^4}-\frac{u_{\sigma}^{eq}\cdot u_{\sigma}^{eq}}{2c_s^2}] \tag{6}$$

where ρ_σ is the density of the σ th component, which can be obtained from $\rho_\sigma = \sum_i f_i^\sigma$. The macroscopic velocity u_σ^{eq} is given by

$$u_\sigma^{eq} = u' + \tau_\sigma F_\sigma / \rho_\sigma \tag{7}$$

where $F_\sigma = F_{c,\sigma} + F_{ads,\sigma} + F_{e,\sigma}$ is the total force acting on the σ th component including fluid-fluid interaction $F_{c,\sigma}$, fluid-solid interaction $F_{ads,\sigma}$ and external force $F_{e,\sigma}$. u' is a velocity common to the various components defined as

$$u' = \sum_\sigma \frac{\rho_\sigma u_\sigma}{\tau_\sigma} / \sum_\sigma \frac{\rho_\sigma}{\tau_\sigma} \tag{8}$$

In Shan-Chen model, the fluid-fluid interaction can be expressed as

$$F_{c,\sigma}(x) = -\varphi(x) \sum_{x'} \sum_{\bar{\sigma}} G_{\sigma\bar{\sigma}}(x, x') \varphi(x')(x' - x) \tag{9}$$

where $G_{\sigma\bar{\sigma}}(x, x')$ is the Green's function which satisfies $G_{\sigma\bar{\sigma}}(x, x') = G_{\sigma\bar{\sigma}}(x', x)$. $\varphi(x)$ is called "effective density" of the σ th component which is defined as a function of the local particle density. Different forms of $\varphi(x)$ lead to different equations of state.

In its original form in Shan-Chen model, the interaction range is defined over the nearest on a hexagonal lattice, i.e.

$$G_{\sigma\bar{\sigma}} = \begin{cases} G, |x' - x| = c \\ 0, |x' - x| > c \end{cases} \tag{10}$$

By projecting from four dimensional (4D) FCHC lattice, the interaction was extended to the next nearest neighbours on a cubic lattice in three dimensions (3D) (Martys and Chen, 1996). In a similar way, the next nearest can also be used in the force discretization in D2Q9 model. According, Eq. (10) is modified to account for the nearest and nest nearest neighbour as

$$G_{\sigma\bar{\sigma}} = \begin{cases} G, |x' - x| = c \\ G/4, |x' - x| = \sqrt{2}c \\ 0, otherwise \end{cases} \tag{11}$$

As shown by (Shan and Doolen, 1996), with the above definition of the interaction potential, the equation of state for D2Q9 lattice-Boltzmann model can be written as

$$P = c_s^2 \rho + \frac{3}{2} G \varphi^2(\rho) \tag{12}$$

This can be considered as the equation of state (EOS) of a non-ideal fluid. The first term on the right-hand side is a kinetic contribution, while the second term is a contribution due to the inter-particle interaction. With interaction potential properly chosen, any equation of state can be modelled. It should be noted that if there is no interaction amongst the same kind of fluid, then the equation of state would reduce to the ideal gas equation of state given by $P = c_s^2 \rho$. In this study, the "effective density" $\varphi(x)$ mentioned above is chosen as $\varphi(x) = \rho_0 [1 - \exp(-\rho / \rho_0)]$, which is commonly used. Other forms of the interaction potential are used and include for example $\varphi = \rho$ (Martys and Chen, 1996); $\varphi = \varphi_0 e^{-\rho_0 / \rho}$ (Sukop and Thorne, 2006). The critical interaction strength will be given by the following two equations

$$\frac{\partial P}{\partial \rho} = 0 \qquad \frac{\partial^2 P}{\partial \rho^2} = 0 \tag{13}$$

In this present study, we choose $\varphi(x) = \rho_0 [1 - \exp(-\rho / \rho_0)]$. This leads to a value of the critical interaction strength to be $G_c = -4/9\rho_0$ for D2Q9 model. Any value of the interaction strength below G_c would result in phase separation.

As the solid-fluid interaction, A method was proposed in (Martys and Chen, 1996) to introduce the interaction force to describe the interaction between a fluid and a wall, which is defined as

$$F_{ads,\sigma}(x) = -G_{ads}\varphi(x)\sum_i s(x')(x'-x) \quad (14)$$

$$G_{ads} = \begin{cases} G_t, |x'-x| = c \\ G_t/4, |x'-x| = \sqrt{2}c \\ 0, otherwise \end{cases} \quad (15)$$

where G_t is the fluid-solid interaction potential parameter, $s(x')$ =0 or 1 for fluid or solid, respectively. By adjusting the interaction strength G_t for each pair of fluid-solid interaction, we control the surface wetting characteristic.

3 Simulation results

3.1 Evaluation of surface tension

The surface tension can be estimated simply by simulating a series of droplets or bubbles of various sizes and measuring their radii and inside/outside pressures. The pressure can be attained by the EOS (Eq. (12)). Then, the pressure difference can be computed. Thus, the surface tension can be calculated according to Laplace's law.

$$\Delta p = \frac{\sigma}{R} \quad (16)$$

The values of pressure and radius are very sensitive to the final results because they are relatively small. Therefore, carefulness is needed when choosing these values in simulating cases. The values of the pressure should be a constant theoretically. However, since the thickness of the interface is finite and both phases exist near the interface, the values of pressure vary near the interface. Therefore, the values of pressure are taken away from the interface where the pressure is almost a constant.

Fig. 1 shows the results agree with Laplace's law very well. For different interaction strength $|G|$ values, the slopes of the lines are different. In another word, different surface tension can be obtained by varying the interaction strength parameter $|G|$. Fig. 2 demonstrates surface tension as a function of $|G|$. It can be seen the surface tension goes up as the interaction strength $|G|$ increases.

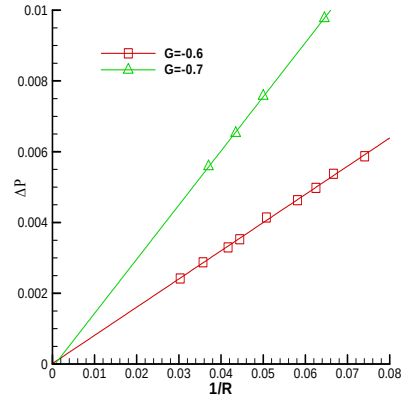

Fig. 1: The pressure difference as a function of its curvature with different $|G|$

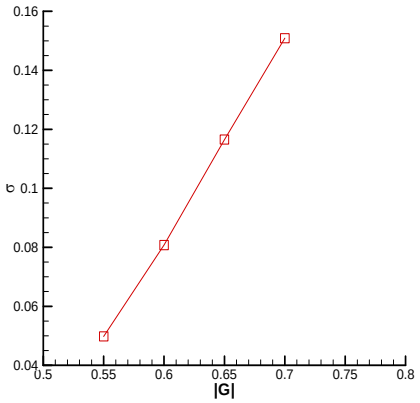

Fig. 2: The surface tension as a function of $|G|$

3.2 Evaluation of fluid-solid interaction

To evaluate the fluid-solid interaction, some simulation cases are carried out. As figure 3(a) shows, a half circle of droplet is initially set on a wall. After the equilibrium status is obtained, different contact angles can be achieved by varying the G_t parameter. Fig. 3 (b), (c) and (d) show three different contact angles θ when fluid-fluid interaction strength G=-0.6, which demonstrates hydrophobic, natural and hydrophilic surfaces.

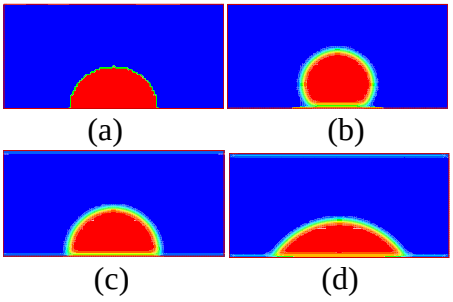

Fig. 3: (a) the initial setting; (b) $\theta = 135°$; (c) $\theta = 90°$; (d) $\theta = 45°$, G=-0.6

Fig. 4 shows the result of the contact angle as a function of G_t. For the three special contact angles of 180°, 90° and 0°, the analytical values of G_t can be obtained via the following equations, respectively

$$\begin{aligned} G_t &= G\varphi_l \\ G_t &= \frac{1}{2}G(\varphi_l + \varphi_v) \\ G_t &= G\varphi_v \end{aligned} \qquad (17)$$

where φ_l and φ_v are the "effective density" of the liquid and vapour phase, respectively. In the present study, we choose $\varphi = 1 - \exp(-\rho)$, G=-0.6, $\rho_l = 2.278$, $\rho_g = 0.118$. Thus, the parameter G_t can be computed. For the three special contact angles are 180°, 90° and 0°, the parameter G_t are -0.1088, -0.3138 and -0.5188, respectively. From the simulation results in figure 7, we can see that when the contact angle is 90°, the parameter G_t is 0.32, which is quite close to the analytical value.

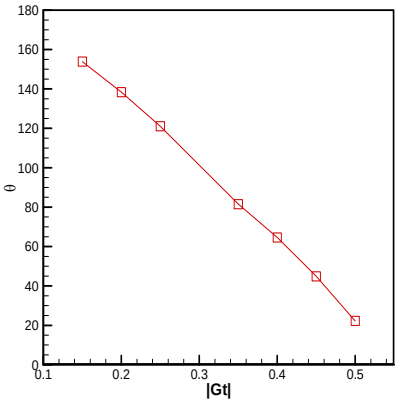

Fig. 4: The contact angle as a function of $|G_t|$, G=-0.6

3.3 Fluid flow in channels

3.3.1 Fluid flow in smooth channel

In this section, simulation of fluid flow through the smooth channel is firstly carried out. A uniform of 1000×50 D2Q9 lattice is applied. The liquid flow is initially filled in the first half channel 500×50 with a speed of u, while gas flow fills the rest channel. Regarding the boundary conditions, periodic boundary condition is applied at the inlet and outlet, while half-way bounce back boundary condition is used at the top and bottom channel. The fluid-fluid interaction strength parameter G is set at -0.6 throughout the simulations. In terms of solid-fluid interaction strength parameter G_t, the range of 0.01-0.4 is investigated. Fig. 5 displays the flows in the channel at t=2500 with different G_t values. It can be seen that the flow with $|G_t|$=0.01 has the longest flow length. Actually, we can see that a gas layer is formed along the channel, which will help to reduce the resistance from the wall. In this study, it is considered as the superhydrophobic channel. However, for the case $|G_t|$=0.45, the channel obviously possess hydrophilic character, where the shortest flow length occurs. In this study, we assume that the longer the flow length is, the better hydrophobicity the channel has.

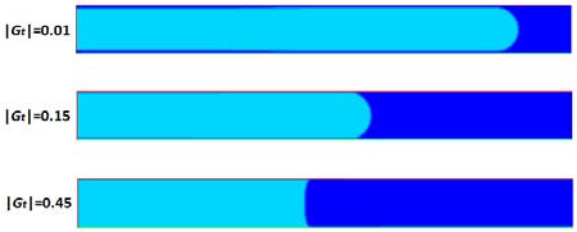

Fig. 5: The flow length in the channel with different $|G_t|$, t=2500

3.3.2 Fluid flow in rough channels

We all know that smooth channel is only the ideal situation. Therefore, in this section, the fluid flow in rough channels is studied. The effect of the style and size of roughness is investigated. Firstly, for the sake of simplicity, the rectangle roughness is patterned along the channel, as shown Fig. 6. In this study, a=4 is use for all simulation cases. Fig. 7 shows the effect of roughness on flow length at t=3000. It can be seen that the roughness helps to reduce the resistance of the channel, hence increase the flow length. We can also find that the increase of flow length with $|G_t|$=0.1 is much less than that of $|G_t|$=0.2. In another word, for the channel that is already superhydrophobic, roughness does not help much. But for the hydrophobic ones, roughness has a chance to make it to be superhydrophobic, which is consistent with the previous experimental works. Actually, most

channels we see in natural word are hydrophobic ones. Also, the roughness has little effect on hydrophilic channels.

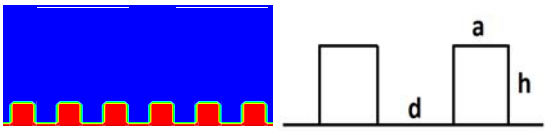

Fig. 6: The structure of rectangular roughness

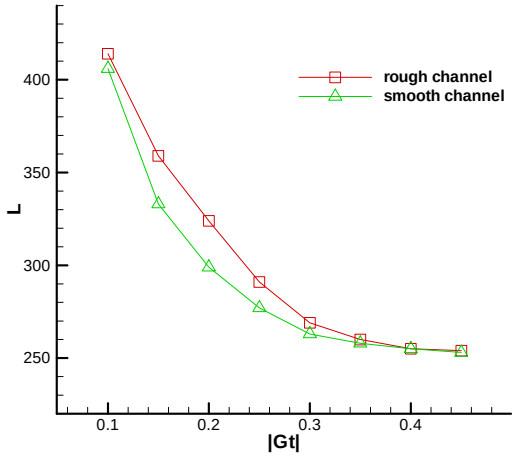

Fig. 7: The effect of roughness on the flow length, t=3000

It is well known that the size of roughness also plays an important role on fluid flow dynamic characters, which will be discussed in detail here. To distinguish the roughness, the ratio of the roughness height and distance h/d is introduced. Fig. 8 and 9 display the effect of roughness with different h/d ratio on flow length. The solid-fluid interaction strength parameter $|G_t|$ is 0.01 in fig. 8, while 0.15 in fig. 9. Different effects can be found for different $|G_t|$ values. To be specific, for the case $|G_t|$=0.01 in fig. 8, the flow length at h/d=0 (i.e. smooth channel) is longer than rough channels. That is to say, for the superhydrophobic channels (in this study, $|G_t|$=0.01), roughness does not contribute to the hydrophobicity. On the contrary, it reduces the hydrophobicity of the channel. It also can be seen that the flow length decreases as h/d increases at the beginning stage, reaching the shortest flow length at h/d=0.25. As the value of h/d increases after that, the flow length increases. It also should be noted that the flow length is almost constant when the ratio h/d>0.8, slightly below the value in smooth channel.

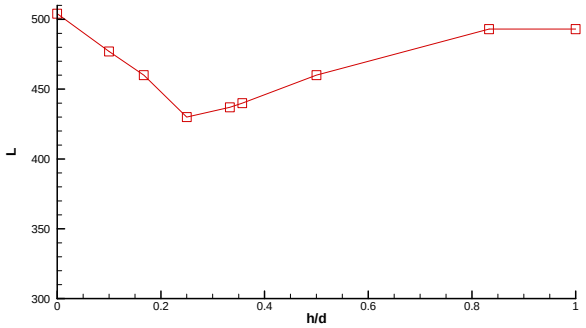

Fig. 8: The flow length in rough channel as a function of the ratio h/d, G_t=-0.01, t=2000

Fig. 9 illustrates the effect of roughness with different h/d on the hydrophobic channel ($|G_t|$=0.15). Considering of the limitation of the actual material's surface free energy, most channels cannot reach superhydrophobic level without the help of roughness. Therefore, this study case more likely accords with the practical applications. From the figure, we can see that roughness mostly contributes to the hydrophobicity for most h/d values. It should be noted that when the ratio h/d is smaller than 0.3, the roughness plays a role of resistance. As the increase of the ratio h/d in the beginning, the flow length increases notably. But later for h/d>0.6, the flow length almost remains a constant. In another word, when the ratio h/d increases (>0.3), the rectangle roughness can increase the hydrophobicity of the channel greatly. The hydrophobicity reaches its maximum when h/d is around 0.6. After that, a bigger ratio of h/d does not help to increase the hydrophobicity. It should be mentioned that the ratio h/d as large as 1.0 is studied. This is based on two considerations. One is when the ratio h/d is larger than 0.6, the effect of the ratio on hydrophobicity almost stays at the same level. The other is that too large ratio will become unreasonable when considering the patterned roughness in the practical application. Nevertheless, the simulation results in this paper should offer some instructions for designing more hydrophobic channels by patterning roughness on the channel surfaces.

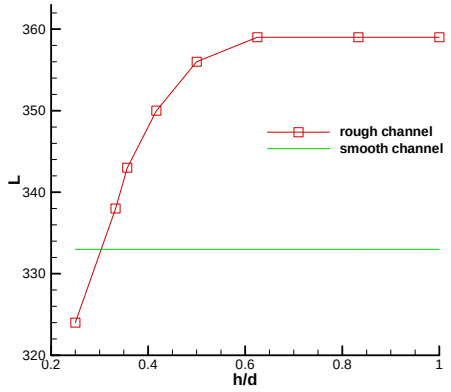

Fig. 9: The flow length in rough and smooth channel as a function of the ratio h/d, G_t=-0.15, t=2500

It can be seen from fig. 9 that rectangular roughness has a limitation to help to increase the hydrophobicity. Actually, to design superhydrophobic channel, more complex roughness is usually needed. Therefore, hierarchical roughness is introduced and investigated here. Fig. 10 displays the structure of the hierarchical roughness that we studied in this paper. To compare with the rectangular roughness, the height h and the distance d are set with h=5, d=6, respectively. The second level of hierarchical roughness is set with a=1, b=2 and c=3. To investigate the effect of hierarchical roughness on hydrophobicity, the fluid flow through the channel with the hierarchical roughness, tow kinds of rectangular roughness (h/d=5/6 and 2/6) and smooth channel are compared. These two sizes of rectangular roughness are chosen is based on the consideration, for hierarchical roughness, h=5 and h-c=2.

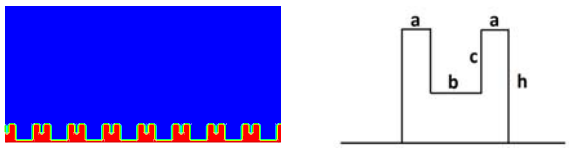

Fig. 10: The structure of hierarchical roughness

The simulation results of the comparison of the four kinds of channel mentioned before are shown in fig. 11. Rough channel 1 represents the channel with rectangular roughness of h/d=5/6, while rough channel for h/d=2/6. It can be seen that, for the solid-fluid interaction parameter $|G_t|$ between 0.1 and 0.2, the hierarchical roughness has the most significant effect on flow length. It means that the hierarchical roughness has a more evident improvement on hydrophobicity compared with the other two kinds of rectangular roughness. Based on this, superhydrophobic channels can be created by patterning hierarchical roughness on hydrophobic channels. It should also be noted that, for hydrophilic channels, the hierarchical roughness plays a strong role of resistance.

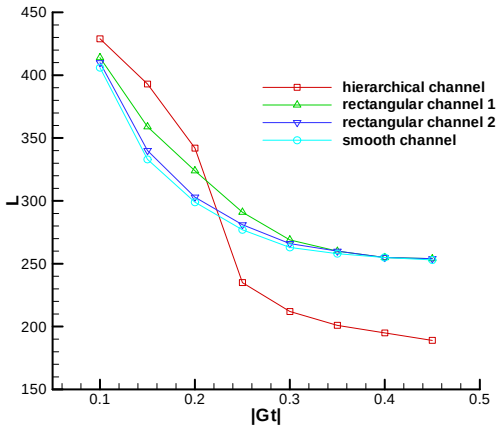

Fig. 11: The flow length in four kinds of channels, t=4000

The frictional resistance coefficient, which is defined by Eq. (17), is also investigated. The smaller the coefficient is, the less the pressure drop is.

$$c_f = 2\Delta pd(|u|^2 \rho l) \qquad (17)$$

Considering the simplicity and no loss of generality, the local frictional resistance coefficient at the same time and position of the channel is studied. Fig. 12 demonstrates the local frictional resistance coefficient at t=2000 and x=L/2 in three kinds of channels. The horizon abscissa 1 stands for the channel with the hierarchical roughness, 2 for h/d=5/6 rectangular roughness and 3 for h/d=2/6 rectangular roughness. It can be seen that the channel with the hierarchical roughness has the smallest frictional resistance coefficient. That is to say, the pressure drop in the channel with hierarchical roughness is the smallest.

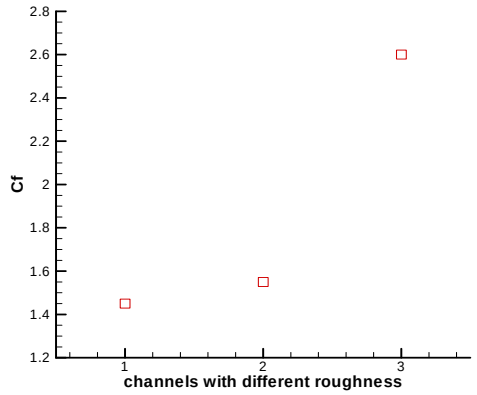

Fig. 12: The frictional resistance coefficient in three kinds of channels, $x=L/2$, $t=2000$

4 Conclusions

In this study, the LBM is employed to investigate the effect of surface roughness on the hydrophobicity of the channel. In particular, the rectangular and hierarchical roughness is studied. For the rectangular roughness, it is found that the ratio of height and the distance h/d has a great effect on hydrophobicity of the channel. To be exact, as the ratio increases, the roughness can help increase the hydrophobicity. However, when the ratio is as large as 0.6, the increasing ratio does not have an evident effect on improving the hydrophobicity. For the hierarchical roughness, the results show that it has greater effect on improving the hydrophobicity of the channel compared with those with rectangular roughness. The simulation results in this study may provide some instructions on designing the superhydrophobic channel by patterning roughness on hydrophobic channels.

Acknowledgment

This work is supported by the UK Royal Society-NSFC (China) International Joint Project (2009-2011), China NSFC under grant (50920105504), and China Scholarship Council (CSC).

References

Chen, S., Doolen, G.D., 1998. Lattice Boltzmann method for fluid flows. Annu Rev Fluid Mech 30, 329-364.

Chibbaro, S., Costa, E., Dimitrov, D., Diotallevi, F., Milchev, A., Palmieri, D., Pontrelli, G., Succi, S., 2009. Capillary Filling in Microchannels with Wall Corrugations: A Comparative Study of the Concus- Finn Criterion by Continuum, Kinetic, and Atomistic Approaches. Langmuir 25, 12653-12660.

Cui, J., Li, W., Lam, W.H., 2010. Numerical investigation on drag reduction with superhydrophobic surfaces by lattice-Boltzmann method. Comput Math Appl.

Dupuis, A., Yeomans, J.M., 2004. Lattice Boltzmann modelling of droplets on chemically heterogeneous surfaces. Future Gener Comp Sy 20, 993-1001.

Gao, N., Yan, Y., 2009. Modeling Superhydrophobic Contact Angles and Wetting Transition. Journal of Bionic Engineering 6, 335-340.

Martys, N.S., Chen, H.D., 1996. Simulation of multicomponent fluids in complex three-dimensional geometries by the lattice Boltzmann method. Phys Rev E 53, 743-750.

Shan, X., Doolen, G., 1996. Diffusion in a multicomponent lattice Boltzmann equation model. Physical Review E 54, 3614-3620.

Sukop, M.C., Thorne, D.T., 2006. Lattice Boltzmann modeling: An introduction for geoscientists and engineers. Springer Verlag.

Yan, Y., Zu, Y., Dong, B., 2010. LBM, a useful tool for mesoscale modelling of single-phase and multiphase flow. Appl Therm Eng.

Yan, Y.Y., 2009. Physical and numerical modelling of biomimetic approaches of natural hydrophobic surfaces. Chinese Sci Bull 54, 541-548.

Yan, Y.Y., Zu, Y.Q., 2007. A lattice Boltzmann method for incompressible two-phase flows on partial wetting surface with large density ratio. J Comput Phys 227, 763-775.

Zhang, J., Kwok, D.Y., 2006. Contact line and contact angle dynamics in superhydrophobic channels. Langmuir 22, 4998-5004.

Zu, Y., Yan, Y., Li, J., Han, Z., 2010. Wetting Behaviours of a Single Droplet on Biomimetic Micro Structured Surfaces. Journal of Bionic Engineering 7, 191-198.